Numerical and experimental investigations on heat/mass transfer of slot-jet impingement in a rectangular cavity

P. W. Li and W. Q. Tao
Department of Power Machinery Engineering, Xi'an Jiaotong University, Xi'an, Shaanxi, The People's Republic of China

Laminar flow and heat/mass transfer of a slot jet impinging in a rectangular cavity are studied numerically and experimentally. The discretization equations are formed by the finite-volume approach. Special attention is paid to the treatment of the outflow boundary condition. The influences of the jet-exit velocity distribution, the distance between the jet exit and the cavity bottom, and the Reynolds number on the local heat transfer distribution of the cavity bottom are investigated. In the experimental work, the local mass transfer coefficient distribution of the bottom surface is measured by the naphthalene sublimation technique. The agreement between the numerical and experimental results is quite satisfactory.

Keywords: jet impingement; naphthalene sublimation; numerical simulation

Introduction

Impingement heat transfer is widely used in many engineering fields, such as cooling of turbine blades, tempering of glassware, drying of paper and textile, etc. In some cases, laminar impinging jets may be encountered, especially when the jet dimensions and the nozzle-to-target distance are small and the fluid is at a high temperature. Information about the local heat transfer coefficient distribution on the impinged surface is of great importance for controlling the technology process and obtaining high-quality products. A number of experimental and theoretical investigations on the heat/mass transfer characteristics of a slot jet impinging normally onto a flat plate were performed by Gardon and Akfirat (1965), Sparrow and Wong (1975), and Miyazaki and Silberman (1972). In all these studies, the impinged plate was designed or assumed to be extended far enough from the stagnation point so that nonplane outflow conditions need not be considered. However, in many practical applications, jet impingement processes proceed in confined spaces. Sparrow and Xu (1987) and Kang and Tao (1989, 1990) conducted experimental studies on mass/heat transfer for circular jet impingement in cone-type cavities. They found that the local heat/mass transfer characteristics of the bottom surface were quite different from those of unconfined flat surface. A search of the literature did not uncover any reference to slot-jet impingement in a rectangular cavity.

In the present study, both numerical and experimental investigations are performed for a slot jet impinging normally onto the bottom of a rectangular cavity. The experimental work aimed at obtaining the local transfer coefficient distribution on the bottom and revealing whether there was a local region on the bottom surface where the three-dimensional (3-D) effect might be neglected. The problem at hand is 3-D in nature; however, our experimental measurement has shown that in the jet midplane, the local mass transfer coefficient distribution of the bottom is characterized by two-dimensional (2-D) behavior. Some of the experimental results will be presented in this paper. Our numerical investigations were performed for a 2-D slot jet, which was supposed to simulate the fluid flow and heat transfer processes at the mid-plane of the 3-D case. The numerical results are compared with the experimental data, and the agreement between them is quite satisfactory.

Experimental apparatus and procedure

An overall diagram of the experimental apparatus is presented in Figure 1. The major part of the apparatus is a large test chamber within which the test section is situated (in Figure 1, the supporter of the test section is shown). The apparatus was operated in a suction mode, with air from the naphthalene-free

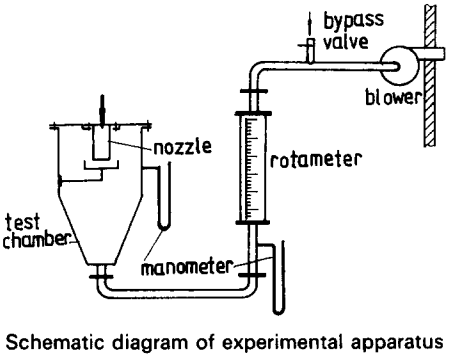

Figure 1 Schematic diagram of experimental apparatus

Address reprint requests to Professor Tao at the Department of Power Machinery Engineering, Xi'an Jiaotong University, Xi'an, Shaanxi 710049, The People's Republic of China.

Received 21 September 1992; accepted 12 January 1993

laboratory room being drawn through the inlet of the jet delivery nozzle. The air passed through the nozzle and emerged as a free jet. After impinging on the bottom naphthalene surface of the test section, the air turned around and flowed along the lateral surface, where further mass transfer took place between the lateral surface and the fluid. The air was then merged into the chamber and conducted to an air-handling system consisting of a rotameter, a control valve, and a blower. The naphthalene-laden charge from the blower was vented outside the building.

A pictorial view of the test section is shown in Figure 2. In order to measure the local transfer coefficients for both the bottom and the lateral surfaces, the test section consisted of five separable parts, one bottom and four pieces of lateral surface. Each part was made of aluminum alloy with one of its lateral surface planes excavated up to a 4 mm depth. The excavated space was filled with naphthalene during a casting process. A cross-sectional view of one piece of the lateral wall is shown in Figure 2b. The dimensions of the test section were as follows:

$a = 67.7$ mm, $b = 50.8$ mm, $c = 14.3$ mm ($a/b = 4/3$, $a/c = 4.7/1$)

These dimensions were adopted by referring to the configuration of a flat commercial TV screen. The jet nozzle was a rectangular duct. It had a length of 80 mm, and its cross-sectional dimension was 4 × 40 mm.

Highly localized measurements of the mass transfer rates were implemented with the aid of a stylus-type gauge. It was a linear variable differential transformer that could provide 0.2 mm linear range and 0.5×10^{-3} mm resolution. This resolution was about two orders of magnitude smaller than the operating range of the measured naphthalene sublimation. The data of the surface profile were recorded by a HP 3054 data acquisition system. The total sublimation amount of naphthalene during a data run was also determined with an analytical balance having a resolution of 0.0001 g and a capacity of 200 g. Measurement of the naphthalene surface profiles were taken before and after each data run. The change in naphthalene depth was determined by differencing the two measured surface elevations at given position. The total sublimation amount was then obtained by numerical integration.

The casting process and the experimental procedures of the naphthalene sublimation technique are well documented in Sparrow et al. (1983) and Xiao and Tao (1990) and will not be restated here. Detailed description of the local measurement process was given in Chyu (1985) and Li (1991).

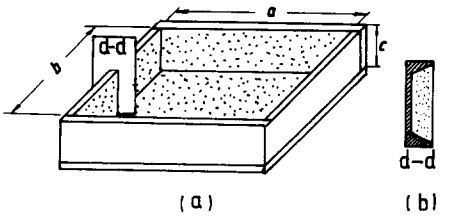

Figure 2 (a) Test section; (b) cross section of one piece of the lateral wall

Data reduction

Mass transfer results are presented in dimensionless form in terms of the Sherwood number, which is defined as

$$\mathrm{Sh} = KB/D \tag{1}$$

where B is the nozzle width (4 mm), which is used as the characteristic length of the Sherwood number.

The diffusion coefficient D is related to the Schmidt number Sc via $D = \nu/\mathrm{Sc}$; thus Equation 1 becomes

$$\mathrm{Sh} = (KB/\nu)\mathrm{Sc} \tag{2}$$

where ν is the kinematic viscosity of air. The value of the air viscosity was determined according to the air temperature and pressure in the test chamber.

The mass transfer coefficient K is calculated by following equation:

$$K = (\Delta M/\tau A)/(\rho_{nw} - \rho_{nj}) \tag{3}$$

where ΔM is the corrected change of naphthalene mass during the data run, for which the extra loss of naphthalene during auxiliary operation was excluded. The naphthalene vapor density at the exit of the nozzle, ρ_{nj}, equals zero for the present study. To determine the naphthalene vapor density at the surface, ρ_{nw}, the naphthalene vapor pressure–temperature relation given by Sogin (1958) was used in conjunction with

Notation

a	Thermal diffusivity of fluid; long-side length of cavity bottom surface
A	Area
b	Short-side length of cavity bottom surface
B	Width of slot-jet nozzle
B_W	Thickness of jet nozzle wall
c	Height of cavity lateral wall
D	Mass diffusion coefficient
H	Distance from jet exit to cavity bottom surface
H_B	Height of lateral wall of two-dimensional cavity
K	Mass transfer coefficient
ΔM	Corrected mass loss of naphthalene during data run
Nu	Nusselt number
p	Pressure
Pr	Prandtl number
Re	Reynolds number
Sc	Schmidt number
Sh	Sherwood number
T	Temperature
u, v	Velocity components in x- and y-direction
V	Average velocity
W_B	Width of two-dimensional cavity
x, y	Cartesian coordinates

Greek symbols

δ	Thickness
ν	Fluid viscosity
ρ	Density
τ	Time duration

Subscripts

b	Bottom
i	Local
j	Jet exit
l	Lateral
n	Naphthalene
s	Stagnation point
w	Wall

the perfect gas law. In SI units, the equation for determining ρ_{nw} is as follows:

$$\rho_{nw} = \frac{10^{(13.564 - 3729.4/T_w)}}{RT_w} \tag{4}$$

where the gas constant R is taken as 64.849 J/(kg.K).

The local amount of sublimation ΔM_i is obtained via the local depth change at that location:

$$\Delta M_i = \rho_n \delta_i \Delta A_i \tag{5}$$

The local mass transfer coefficient K_i is then obtained from the following equation:

$$K_i = \rho_n \delta_i / (\tau(\rho_{nw} - \rho_{nj})) \tag{6}$$

The jet Reynolds number is evaluated as that of the air flow exiting the jet nozzle, i.e.,

$$\mathrm{Re} = V_j B/\nu \tag{7}$$

Mathematical model

In this section a 2-D model of the jet impingement problem described above will be formulated. The 2-D case will be solved for the heat transfer process. According to the heat/mass transfer analogy theory (Eckert 1976), sublimation on a naphthalene surface corresponds to the heat transfer on a isothermal surface, with the fluid Prandtl number being equal to the Schmidt number.

A schematic diagram that depicts the problem to be analyzed is presented in Figure 3. A parallel-plate channel (i.e., nozzle) of width B and wall width B_w conveys a laminar flow to its exit plane, which is situated at a distance H from the bottom surface of the cavity. The jet with temperature T_j at the channel exit impinges onto the rectangular cavity whose inner surface temperature is T_w. The bottom of the cavity has a width of W_B. The lateral height of the cavity is H_B, which may be higher than, equal to, or lower than H. Since the physical model is symmetric, only half of the flow field is taken as the calculation domain (see Figure 4). It is assumed that the flow and heat transfer are in steady state and the fluid physical properties are constant.

The governing equations of the problem described are as follows:

$$\frac{\partial u}{\partial x} + \frac{\partial v}{\partial y} = 0 \tag{8}$$

$$u\frac{\partial u}{\partial x} + v\frac{\partial u}{\partial y} = -\frac{1}{\rho}\frac{\partial p}{\partial x} + \nu\left(\frac{\partial^2 u}{\partial x^2} + \frac{\partial^2 u}{\partial y^2}\right) \tag{9}$$

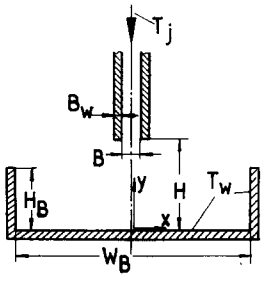

Figure 3 Configuration of numerical simulation

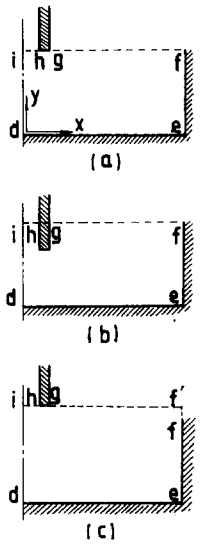

Figure 4 Three cases of computation domain. (a) H = HB; (b) H < HB; (c) H > HB

$$u\frac{\partial v}{\partial x} + v\frac{\partial v}{\partial y} = -\frac{1}{\rho}\frac{\partial p}{\partial y} + \nu\left(\frac{\partial^2 v}{\partial x^2} + \frac{\partial^2 v}{\partial y^2}\right) \tag{10}$$

$$u\frac{\partial T}{\partial x} + v\frac{\partial T}{\partial y} = a\left(\frac{\partial^2 T}{\partial x^2} + \frac{\partial^2 T}{\partial y^2}\right) \tag{11}$$

The boundary conditions of the three computation domains shown in Figure 4 are as follows:

$$\text{On } i\text{–}d\text{: } (x = 0,\ 0 \le y \le H),\ u = 0,\ \frac{\partial v}{\partial x} = 0,\ \frac{\partial T}{\partial x} = 0 \tag{12a}$$

$$\text{On } d\text{–}e\text{: } (0 \le x \le W_B/2,\ y = 0),\ u = 0,\ v = 0,\ T = T_w \tag{12b}$$

$$\text{On } e\text{–}f\text{: } (x = W_B/2,\ 0 \le y \le H_B),\ u = 0,\ v = 0,\ T = T_w \tag{12c}$$

$$\text{On } h\text{–}i\text{: } (0 \le x \le B/2,\ y = H),\ u = u(x),\ v = v(x),\ T = T_j \tag{12d}$$

$$\text{On } g\text{–}h\text{: } (B/2 \le x \le B/2 + B_W,\ y = H),\ u = 0,\ v = 0,\ T = T_j \tag{12e}$$

At the outlet boundary f–g (for Figure 4a and 4b) and f'–g (for Figure 4c), where $(B/2 + B_W) \le x \le W_B$, and $y = H$, the following boundary conditions are assumed:

$$\frac{\partial u}{\partial y} = 0\ \frac{\partial u}{\partial x} + \frac{\partial v}{\partial y} = 0\ \left.\frac{\partial T}{\partial y}\right|_{v \ge 0} = 0,\quad \left. T \right|_{v < 0} = T_j \tag{12f}$$

At the outlet boundary f–f' (for Figure 4c), where $x = W_B/2$ and $H_B < y \le H$, the boundary conditions are

$$\frac{\partial v}{\partial x} = 0\ \frac{\partial u}{\partial x} + \frac{\partial v}{\partial y} = 0\ \left.\frac{\partial T}{\partial x}\right|_{u \ge 0} = 0,\quad \left. T \right|_{u < 0} = T_j \tag{12g}$$

A discussion will be given in the next section about the outlet boundary conditions.

Numerical method

The main issue to be dealt with in this section is the treatment of the outlet boundary condition. Before discussing this, the numerical algorithm to solve the problem will be briefly introduced.

The governing equations 8–11 were discretized using the finite-volume approach (Patankar 1980). The SIMPLE algorithm was used to deal with the linkage between the

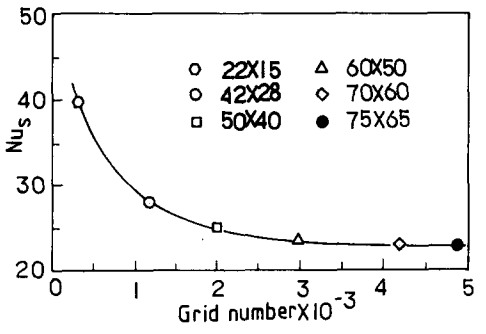

Figure 5 Examination of grid independence of numerical solution

pressure and the velocity. The staggered grid arrangement was used. The convection–diffusion terms in the momentum and energy equations were discretized by the power-law scheme (Patankar, 1980). The resulting algebraic equations were solved by the SLUR method incorporated with the block correction technique.

Attention is now turned to the treatment of the outflow boundary condition. The conventional practice for the treatment of the outflow boundary (Patankar, 1980) is to assume local one-way behavior for the outflow, which makes the corresponding coefficient in the discretization equation of the control volume neighboring the boundary zero; hence no boundary values are needed. However, this practice is appropriate only for the situation when no recirculating flow occurs in the outflow region. As mentioned above, in the present study the distance between the cavity bottom and the jet exit plane may be larger than the height of the cavity lateral wall (Figure 4c). For this case, at the boundaries f–f' and f'–g, mass and momentum exchange must occur between the fluid inside the cavity and that outside of the cavity. For the cases of Figures 4a and 4b, those exchanges are also likely to occur across the boundary g–f. Therefore, for the problem studied, the one-way-behavior assumption is not appropriate.

The outflow boundary conditions set up in the preceding section are based on the following considerations. Since the velocity component parallel to the outflow boundary makes no contribution to the exchanges of mass and momentum between the fluids inside and outside the computation domain, the gradient of this velocity component is assumed to be zero across the boundary. The other velocity component is normal to the outflow boundary and, therefore, is the major contributor to the mass and momentum exchanges across the boundary. In the numerical computation, at the end of each iteration level, its value at the outflow boundary was determined by the continuity equation and was adopted as the boundary value for the next iteration. As far as the fluid temperature is concerned, it may take the value of the inner point (normal velocity is from inside to outside) or the value of T_j (normal velocity is from outside to inside). Here it is assumed that the ambient temperature is approximately equal to the jet exit temperature.

In the following, the problem parameters, the grid network, and the convergence criteria will be briefly addressed. There are six dimensionless parameters in this problem, i.e., W_B/B, H_B/B, B_W/B, Pr, H/B, and Re. In the present study, the first four parameters were fixed. Their values are

$$W_B/B = 12.5,\ H_B/B = 3.58,\ B_W/B = 0.5,\ \mathrm{Pr} = 2.5$$

The values of W_B/B and H_B/B were selected by referring to the configuration of a commercial TV screen. The value of the Prandtl number was taken from that of the Schmidt number in the naphthalene sublimation technique. The nozzle width B was taken as the characteristic length for Reynolds number and Nusselt number. The temperature difference ($T_w - T_j$) was used in the calculation of the heat transfer coefficient.

The grid points in the x- and y-directions were distributed in a nonuniform manner with a higher concentration of grids close to the wall. In order to ensure the grid independence of the numerical solutions, a preliminary computation was performed with six grid systems for the case of Re = 942 and $H/B = 3.58$. The predicted Nusselt numbers are shown in Figure 5. As seen there, starting from the grid system of 60 × 50, the Nusselt number at the stagnation point ceases changing. It was found that the average Nusselt number of the bottom surface was less sensitive to the grid number than that of the stagnation point. To keep a reasonable accuracy and save computation time, a grid system of 50 × 50 was adopted for all the computations.

The convergence criteria for the iterative solution procedure include the following indexes: the maximum percentage difference of two successive iterations in u and v was less than 10^{-4}, the maximum percentage difference in T was less than 10^{-6}, and the ratio of the mass residual in the computation domain to the total flow rate was less than 10^{-6}.

Results and discussion

In order to make a compact presentation, the numerical and experimental results will be presented in a comparative manner whenever possible. The first part of the presentation will be the local measurement results of the bottom surface.

A contour map of the measured local Sherwood number of the bottom surface is shown in Figure 6 for the case of Re = 942 and $H/B = 1.0$. In the figure, only the upper half of the bottom surface and the lower half of the jet nozzle are presented. The lower half of the bottom-surface contour map is basically symmetric to the upper one, and therefore is not shown in the figure. From the figure the following features may be noted. First, in the central region of the bottom surface, the contour lines are basically a series of narrow rectangles with two vertical curved sides, reflecting the configuration of the nozzle exit cross section. Second, in a not too narrow region around the midline 1–1, all contours are almost parallel to each other, indicating the 2-D character of the physical process. The width of this 2-D region is about one third the length of the long side of the nozzle. The 3-D behavior gradually becomes significant with the increase in x-coordinate. In the regions near the two ends of side a, the fluid flow and heat transfer are fully 3-D. This observation of the local Sherwood number distribution on the bottom surface gives us a strong support on using a 2-D model

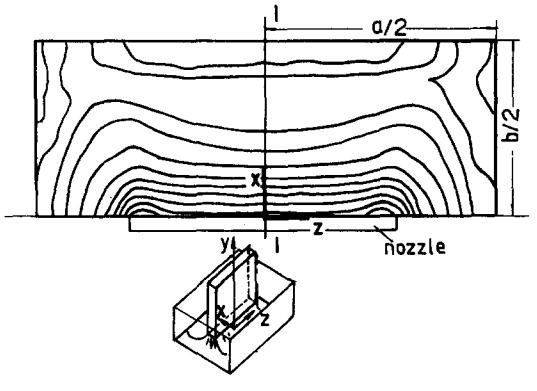

Figure 6 Contour map of Nusselt number of bottom surface (Re = 942, $H/B = 1.0$)

to simulate the transfer process in the region around the midline 1–1. The subsequent presentations are all focused on the 2-D behavior of the numerical and experimental results.

The numerical results of the effect of the jet exit velocity distribution on the local Nusselt number distribution of the bottom surface are now addressed. This examination was conducted with three distribution patterns: uniform, fully developed, and semi-fully-developed. The semi-fully-developed pattern of the jet exit velocity was obtained via numerical computation with a ratio of an entrance length to the nozzle width of 25, which corresponded to the experimental condition. The predicted Nusselt number distributions are shown in Figure 7. As seen there, at a fixed mass flow rate, the effect of the nozzle exit velocity distribution on the local Nusselt number is mainly restricted in a narrow region around the stagnation point, where the Nusselt number corresponding to the fully developed distribution is about 1.7 times that corresponding to the uniform distribution. As expected, the Nusselt number corresponding to the semi-fully-developed distribution is between the above two. Obviously, the difference in Nusselt number at the stagnation point is the result of the difference in impinging velocity for the same flow rate. Since the semi-fully-developed flow pattern corresponds to our experimental condition, all the other computations were performed with this distribution.

Attention is now turned to the variation of the local Nusselt number along the x-axis. In Figure 8 both numerical and experimental results are presented for four cases. It can be seen that the variation patterns of the local Nusselt number along the x-axis at different values of H/B are more or less the same, and the agreement between the numerical and experimental results is quite satisfactory. The Nusselt number has its highest value at the stagnation point, and then rapidly decreases with the increase in x. Starting from x/W_B about 0.2, the local Nusselt number almost keeps constant in a short distance. From x/W_B about 0.3, it increases with x quite appreciably, reaches its second maximum, and then goes down again. It should be noted that for the case of Re = 942, no local measurement data at points closer to the corner were obtained. However, in another series of experiments that were specially designed for comparison with different treatment of the outflow boundary conditions and were performed at different Reynolds number and H/B values, measurements were carried out at two more locations between $x/W_B = 0.45$ and $x/W_B = 0.5$, and these data definitely showed the decreasing trend of the local Sherwood number when x/W_B approached 0.5. This variation pattern of the local Nusselt number is quite different from that of jet inpingement onto an unconfined surface, for which the local Nusselt number decreases monotonically with increase in the distance from the stagnation point. It is considered that

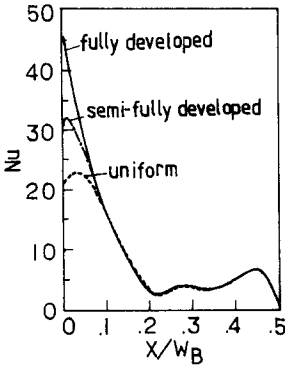

Figure 7 Effect of jet exit velocity distribution. (Re = 942, H/B = 3.58)

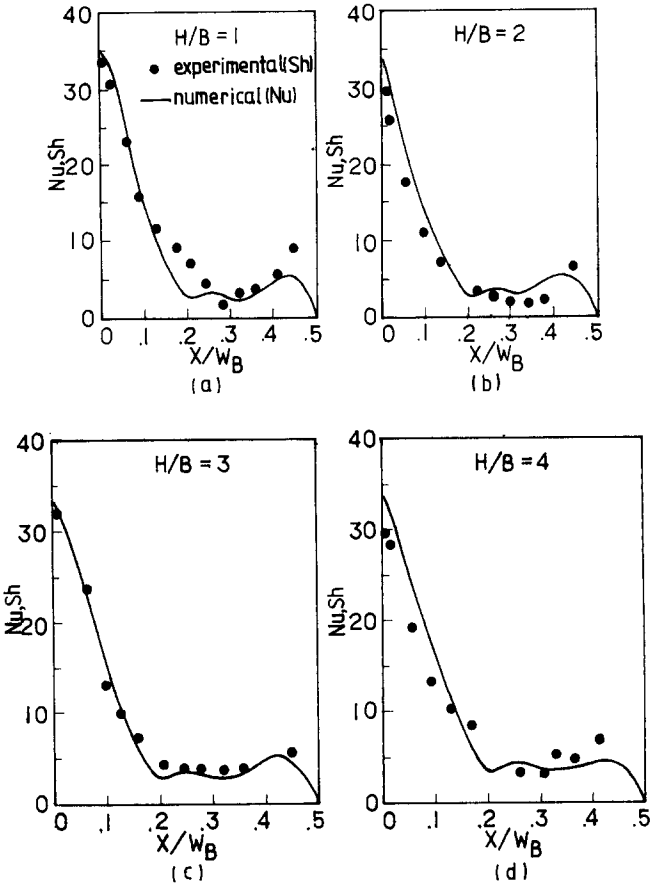

Figure 8 Local Nusselt (Sherwood) number distribution. (Re = 942). (a) $H/B = 1$; (b) $H/B = 2$; (c) $H/B = 3$; (d) $H/B = 4$

this variation pattern is caused by the obstacle effect of the lateral wall of the cavity, which causes a recirculating flow around the corner. This will be seen clearly from the predicted streamlines and the velocity vector distribution shown later. The research on the effect of different outflow boundary conditions has produced a superabundance of results that cannot be presented in a paper confined to journal length limitations. Therefore, these results will be presented elsewhere.

From the results shown in Figure 8, it may be observed that the average Nusselt number of the bottom surface is not sensitive to the parameter H/B. Our numerical computations conducted for other three values of H/B (i.e., $H/B = 3.58$, 5, and 6) yielded the same results. The average Nusselt number of the bottom surface at different values of H/B and fixed Reynolds number are presented in Figure 9. It should be noted that the insensitivity of the bottom Nusselt number to H/B is a unique character of the heat/mass transfer processes proceeding in a cavity at low Reynolds number. In Sparrow and Xu (1987) and Kang and Tao (1989, 1990) it has been demonstrated by naphthalene sublimation experiments that for jet impingement in a cylindrical cavity at Reynolds number 10^4, the curve of the average bottom Sherwood number with H/B is of the convex type, for which at some value of H/B a maximum Sherwood number occurs.

The effect of the Reynolds number on the bottom heat transfer is now examined, and Figure 10 is presented for this purpose. It can be seen from the figure that with the increase in the jet exit Reynolds number, not only the value of the Nusselt number but also its distribution pattern is affected. For the case of Re = 1,900, there are three peaks on the local Nusselt number distribution curve. One peak is at the

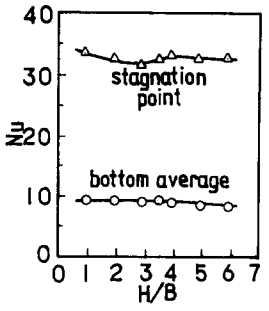

Figure 9 Computational results of effect of H/B on Nusselt number (Re = 942)

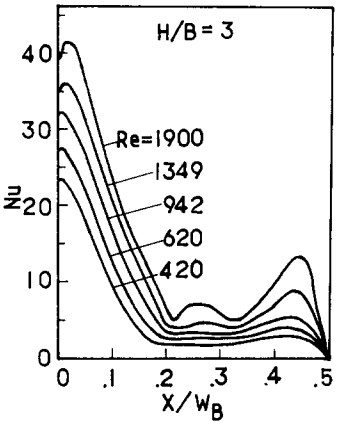

Figure 10 Computational results of effect Reynolds number on bottom-surface heat transfer ($H/B = 3$)

stagnation point, the second is mid-way between the stagnation point and the lateral wall, and the third is near the lateral wall of the cavity. The latter two peaks result from the recirculating flow near the lateral wall. This will be described below.

Attention is now turned to the predicted streamlines and isotherms. In Figures 11 and 12, the isotherms, streamlines, and velocity vector distributions are presented for two cases. From these figures, the following features may be noted. First, in the vicinity of the stagnation point, there exist temperature and velocity boundary layers on the solid surface, in which the velocity distribution is of skewed parabolic type. This boundary-layer region extends to about two fiths of the half-width of the bottom surface. With increase in distance from the stagnation point, the boundary layers are forced to separate from the bottom surface by the recirculating flow formed in the vicinity of the lateral wall. The existence of the boundary-layer flow around the stagnation point is responsible for the high heat transfer coefficient in this region. Second, in the region of x/W_B about 0.2 to 0.3, there are two streams with opposite flow direction along the surface; one stream is the boundary-layer flow that is deviating from the surface, and the other is the recirculating flow bouncing off the lateral wall. It is the effect of these two opposite-direction fluid streams that makes the heat transfer coefficient in this region stay almost constant. Third, careful inspection of the two figures for velocity vector distribution (Figures 11b and 12b) reveals some differences in the recirculating flow region for the two cases. At a Reynolds number of 970, only one circulation is formed, while for Re = 1,700, a second recirculating flow occurs in the vicinity very close to the corner. That is why, at higher Reynolds numbers, the Nusselt number distribution curve has two peaks in the recirculating zone; the large recirculating flow is responsible for the peak midway between the stagnation point and the lateral wall, while the small vortex causes the other peak.

Finally, correlations of the Nusselt number with Reynolds number are provided. The variation of the average Nusselt number of the bottom and the lateral wall with the jet exit Reynolds number can be well fitted by the power-law equation. As an example, in Figure 13 three curves are presented for the case of $H/B = 3$. These three equations are

$$\mathrm{Nu}_s = 3.185\mathrm{Re}^{0.333} \tag{13}$$

$$\mathrm{Nu}_b = 0.126\mathrm{Re}^{0.625} \tag{14}$$

$$\mathrm{Nu}_1 = 0.008\mathrm{Re}^{0.918} \tag{15}$$

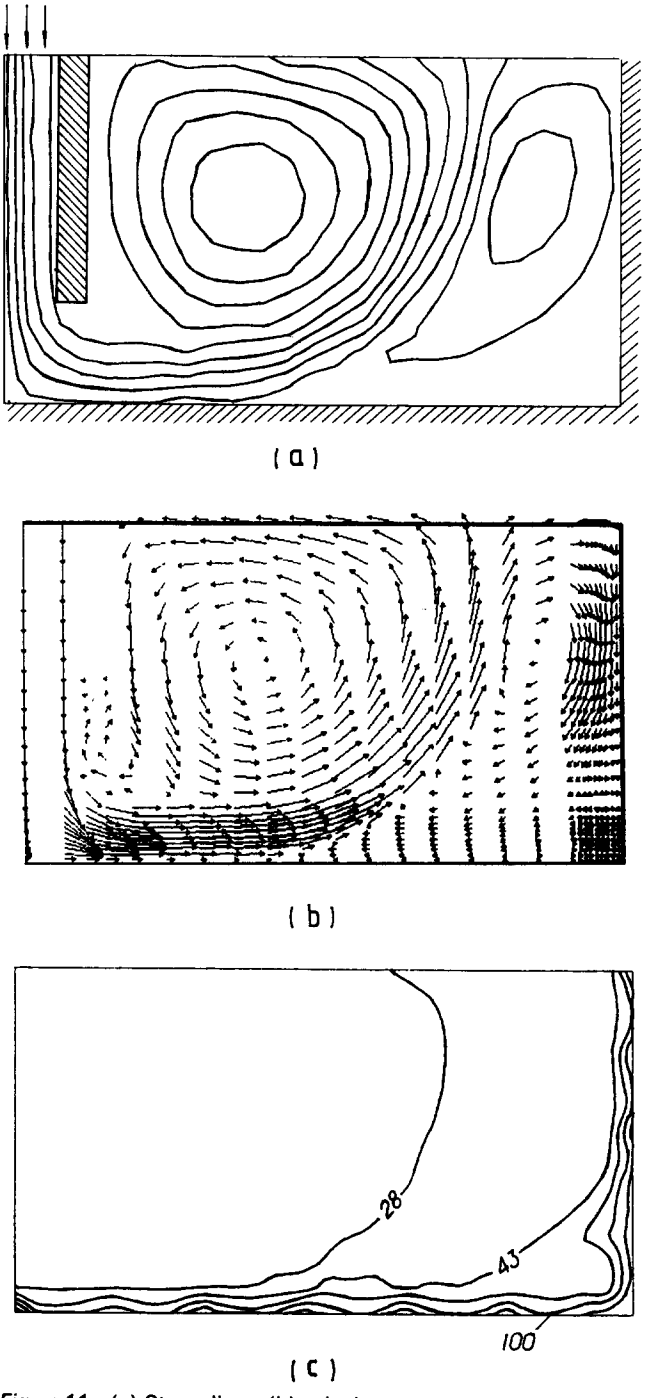

Figure 11 (a) Streamlines, (b) velocity vector distribution, and (c) isotherms (Re = 970, $H/B = 2$)

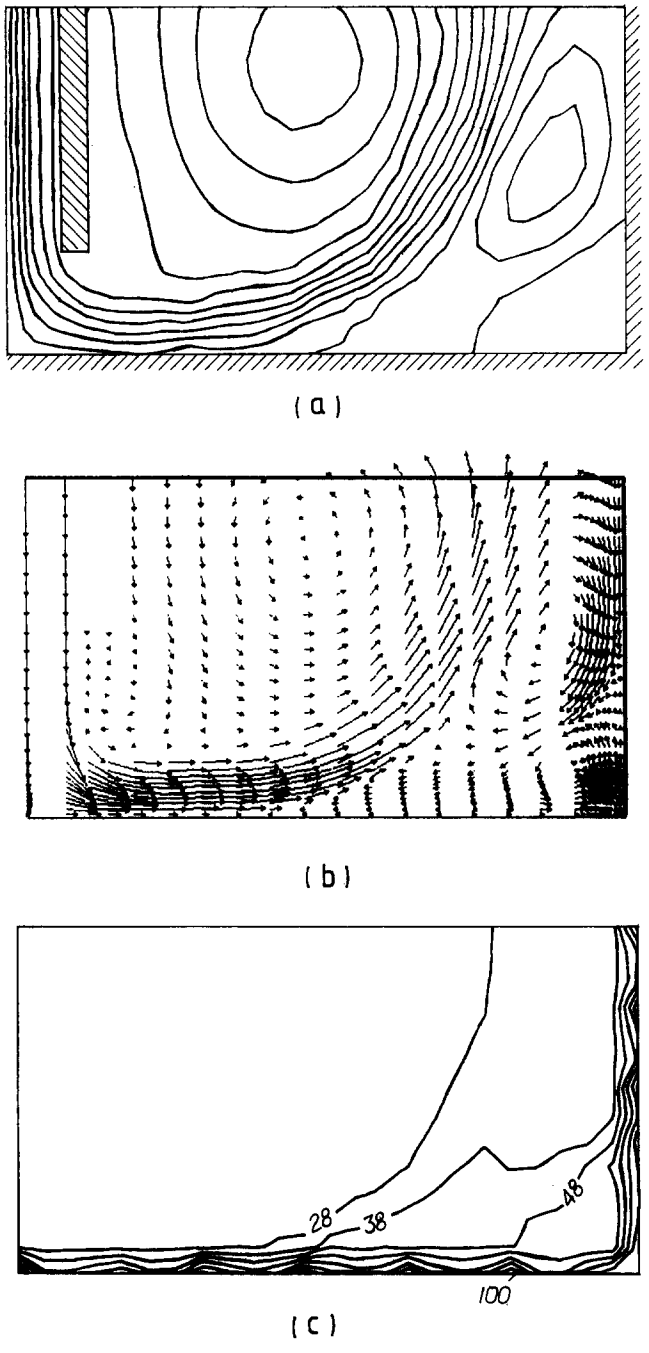

Figure 12 (a) Streamlines, (b) velocity vector distribution, and (c) isotherms (Re = 1700, $H/B = 2$)

It can be seen that the slopes of the three curves are quite different. This may be understood from the level of heat transfer intensity at the different locations. For the problem analyzed in this paper, the highest heat transfer intensity occurs at the stagnation point, while the heat transfer on the lateral wall is relatively weak. Therefore, the increase in Reynolds number has a more significant effect on the enhancement of heat transfer on the lateral wall than does the stagnation point. It should be noted that Equation 14 also can be used for other H/B cases. As noted earlier, the effect of H/B on the average Nusselt number of the bottom surface is very weak.

It is interesting to note that the exponents of Re in Equations 13 and 14 are consistent with the experimental results (Martin 1977), which were performed for slot-jet impingement on an unconfined flat surface. It is stated there that in the Reynolds number range from 3,000 to 90,000, the exponent of Re in the equation for the average Sherwood number varies from 0.56 to 0.68. It should be noted that the characteristic length of Re in Martin (1977) is $2B$; hence, this variation range corresponds to 1,500 to 45,000 when B is used as the characteristic length. No correlation for the local Sherwood number at the stagnation point was provided in Martin (1977). However, with careful inspection the local measurement results for Re = 2,900 and 5,800 presented in Figure 5 of Martin (1977), it is found that the percentage variation of the local Sherwood number at the stagnation point is appreciably less than that of most of the other measurement locations. This indicates that the exponent of Re for the stagnation point should be less than that for the average results of the surface.

Conclusions

In this paper, the results of numerical and experimental studies on the laminar slot-jet impingement heat transfer in a rectangular cavity have been presented. In the numerical work, special attention has been paid to the treatment of the outflow boundary conditions, and the results presented here are all based on the use of the mass conservation law at the exit boundary. The experimental work has been implemented by the naphthalene sublimation technique, and the local Sherwood number distributions have been measured for a series of values of H/B. Experimental results have shown that in the central part of the bottom surface, the heat/mass transfer and fluid flow are 2-D in essence. The local Nusselt number distribution predicted by a 2-D model has agreed well with the measured results on the midline of the bottom surface.

Both numerical and experimental results have shown that with the increase in x/W_B, apart from the first peak at the stagnation point, a second or third peak occurs on the Nusselt number distribution curve, which results from the recirculating flow. Numerical prediction has shown that from Re about 1,400, a second vortex is formed in the recirculating zone, which is responsible for the third peak on the Nusselt number distribution curve.

The effect of the jet exit velocity distribution has been revealed by numerical simulation. It has been found that the effect is mainly restricted to a small region around the stagnation point. Although the difference in the stagnation-point Nusselt number corresponding to the fully developed and

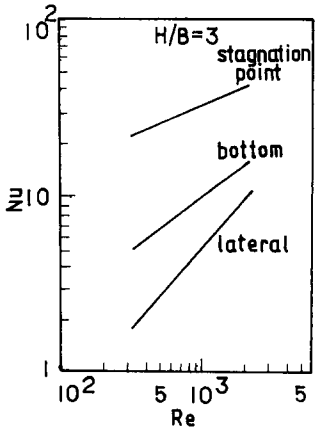

Figure 13 Nusselt number vs. Reynolds number (numerical results)

uniform distribution of the jet exit velocity may be as large as 70 percent, the difference outside this region is totally negligible.

The configuration studied is characterized by a low lateral wall. Both numerical and experimental results have shown that for the configuration studied, the average Nusselt number of the bottom surface is not sensitive to the value of H/B in the range of 1 to 6. This is quite different from the results of jet impingement in a cylindrical cavity with a rather high lateral wall, for which the curve of Sh *versus* H/B is of convex type with a maximum Sherwood number occurring at some intermediate value of H/B.

The relationships of the average Nusselt number with Reynolds number have been well correlated by power-law equations. The correlations for $H/B = 3$ have been provided. It is found that the effect of the jet exit Reynolds number on the lateral wall is much more significant than that on the bottom surface.

Acknowledgment

This work was supported by the National Natural Science Foundation of China.

References

Chyu, M. K. 1986. Influence of roughness element on local mass transfer from flat plate. Ph.D. thesis, University of Minnesota, Minneapolis, MN, USA

Eckert, E. R. G. 1976. Analogies to heat transfer processes. In E. R. G. Eckert and R. J. Goldstein (eds.), *Measurements in Heat Transfer*, Hemisphere, Washington, DC

Gardon, R. and Akfirat, J. C. 1965. The role of turbulence in determining the heat transfer characteristics of impinging jets. *Int. J. Heat Mass Transfer*, **8**, 1262–1272

Kang, H. J. and Tao, W. Q. 1989. Heat/mass transfer for circular jet impingement in a cylindrical cavity with one end open to the ambient air. *AIAA 27th Space Science Meeting*, Reno, NV, USA

Kang, H. J. and Tao, W. Q. 1990. Experimental study of mass/heat transfer for circular jet impingement in a confined conical cavity. *CSET J. Eng. Thermophys.* (in Chinese), **11**, 76–78

Li, P. W. 1991. Experimental and numerical investigations on heat/mass transfer of jet impingement in rectangular cavities. Thesis, Department of Power Machinery Engineering, Xi'an Jiaotong University, Xi'an, Shaanxi, PRC

Martin, H. 1977. Heat and mass transfer between impinging gas jets and solid surfaces. In J. P. Hartnett and T. F. Irvine, Jr. (eds.), *Advances in Heat Transfer*, Vol. 13. Academic Press, New York

Miyazaki, H. and Silberman, E. 1972. Flow and heat transfer on a flat plate normal to a two-dimensional laminar jet issuing from a nozzle of finite height. *Int. J. Heat Mass Transfer*, **15**, 2097–2107

Patankar, S. V. 1980. *Numerical Heat Transfer and Fluid Flow*. Hemisphere, Washington, DC

Sogin, H. H. 1958. Sublimation from disks to air streams normal to their surfaces. *Trans. ASME*, **80**, 61–71

Sparrow, E. M., Tao, W. Q., and Radiky, D. 1983. Heat transfer at an array of co-planar slot-like surface oriented normal to a forced convection flow. *Int. J. Heat Mass Transfer*, **26**, 33–40

Sparrow, E. M. and Wong, T. C. 1975. Impingement heat transfer coefficients due to initially laminar slot jets. *Int. J. Heat Mass Transfer*, **18**, 597–605

Sparrow, E. M. and Xu, Z. X. 1987. Heat (mass) transfer for circular jet impinging on a confined disk with annular collection of the spent air. *ASME J. Heat Transfer*, **109**, 329–335

Xiao, Q. and Tao, W. Q. 1990. Effect of fin spacing on heat transfer and pressure drop of two-row corrugated fin-and-tube heat exchanger. *Int. Comm. Heat Mass Transfer*, **17**, 577–586